AIAA JOURNAL
Vol. 36, No. 12, December 1998

Construction of Response Surface Approximations for Design Optimization

Gerhard Venter* and Raphael T. Haftka†
University of Florida, Gainesville, Florida 32611-6250
and
James H. Starnes Jr.‡
NASA Langley Research Center, Hampton, Virginia 23681-0001

Using response surface approximations for design constraints in design optimization provides the designer with an overall perspective of the system response within the design space. Response surface approximations also reduce the numerical noise inherent in many numerical models and simplify the process of integrating several design codes, as is typically required in multidisciplinary optimization. Procedures are discussed for constructing accurate response surface approximations to represent design constraints in design optimization. Response surface approximations are constructed for the stresses and buckling loads of an isotropic plate with an abrupt change of thickness. These response surface approximations are constructed from numerical experiments conducted with a finite element analysis procedure and are used for minimum-weight optimum design of the plate. Nondimensional variables and stepwise regression are used to reduce the complexity and increase the accuracy of the response surface approximations. Additionally, higher-order polynomials (cubic and quartic instead of the more traditional quadratic) are used as response surface approximations, and a detailed error analysis, using an independent data set, is performed. Finally, it is shown that, by making use of response surface approximations, the optimum weight of the plate may be presented in the form of a design chart for a wide range of geometric, loading, and material constants.

Nomenclature

A	= cross-sectional area of the plate
a	= length of the plate
b	= width of the plate
Cp	= Mallow's Cp statistic
D	= flexural stiffness of the plate
E	= Young's modulus
F, f	= response function
N_{crit}	= buckling load
N_x	= axial load
n	= number of experimental data points
P	= applied load
p	= number of parameters in the response model
r	= radial distance from re-entrant corner
S_ε	= mean sum of squares of the error
t	= thickness of the plate
u, v, w	= displacements in the x, y, and z directions
$\boldsymbol{X}$	= model matrix
X, Y, Z; x, y, z	= plate coordinate system
y	= response variable
z_i	= predictor variables
α, β, γ	= nondimensional variables describing the geometry and location of the change in thickness (see Fig. 2)
δ	= experimental error
ε	= difference between predicted and expected response values
ε_x, ε_z, γ_{xz}	= extensive strains in the x and z directions and corresponding shear strain
ζ	= severity of the stress singularity at the re-entrant corner
η	= mean or expected response
θ	= angle of re-entrant corner
λ_i	= response model coefficients
ν	= Poisson's ratio
σ_x, σ_z, τ_{xz}	= normal stresses in the x and z directions and corresponding shear strain
σ_Y	= yield stress
$\hat{}$	= predicted value
$\bar{}$	= average value
$\tilde{}$	= nondimensional value

I. Introduction

In the past, designers have made use of design charts prepared by specialists to aid them in the design process. Typically, a specialist would produce charts and tables after developing a new analysis technique, and designers could use these design charts without in-depth knowledge of the new technique. Design charts were simple to use and gave the designer an overall perspective of the design tradeoffs associated with design decisions. In contrast, modern optimization procedures rely heavily on computerized analysis techniques. These techniques are more advanced than the earlier design charts, but they require more expertise on the part of the designer. Compared to design charts, modern techniques have several other limitations, most notably that the designer is not provided with an overall perspective of system response. Without this overall perspective, complications may arise within the optimization procedure. For example, Giunta et al.[1] found that numerical noise, inherent in many numerical analysis procedures, created spurious local minima in the design space. Also, modern computational procedures make it possible to include analytical results from more than one technical discipline, but integrating several optimization and analysis software codes is a complex and often frustrating task.[2]

As a result of these problems, there is growing interest in using response surface techniques that provide results that resemble the earlier design charts, especially for multidisciplinary optimization. For example, Mason et al.[3] used response surface approximations

Presented as Paper 96-4040 at the AIAA/NASA/ISSMO 6th Symposium on Multidisciplinary Analysis and Optimization, Bellevue, WA, Sept. 4–6, 1996; received Oct. 2, 1997; revision received June 6, 1998; accepted for publication July 31, 1998. Copyright © 1998 by the authors. Published by the American Institute of Aeronautics and Astronautics, Inc., with permission.

*Graduate Research Assistant, Department of Aerospace Engineering, Mechanics and Engineering Science; currently Senior Research and Development Engineer, Vanderplaats Research and Development, Inc., 1767 South 8th Street, Suite 210, Colorado Springs, CO 80906. E-mail: gventer@vrand.com. Student Member AIAA.

†Professor, Department of Aerospace Engineering, Mechanics and Engineering Science. Fellow AIAA.

‡Head, Structural Mechanics Branch. Fellow AIAA.

for a single discipline optimization problem where it was difficult to connect the analysis and optimization codes. Tai et al.,[4] Giunta et al.,[5] Brown and Nachlas,[6] and White et al.[7] used response surface approximations to address the organizational challenge posed by multidisciplinary optimization, whereas Mistree et al.[8] made extensive use of the overall perspective of the design space that response surface approximations provide. Also, Van Houten et al.[9] showed that response surface methodology is a valuable tool for optimization problems with nonsmooth functions. Thacker and Wu[10] used response surface approximations to reduce the computational cost associated with reliability-based optimization problems, which require a large number of function evaluations.

Many response surface approximations are expressed in terms of polynomials in the design variables. However, Kaufman et al.[2] showed that better accuracy may be achieved by using variables that are intrinsic to the approximated response function. The present paper shows how intrinsic variables can be identified with the aid of a nondimensional formulation of the governing equations. The dimensional analysis of the governing equations is discussed in more detail by Venter et al.[11] High-accuracy approximations are then obtained by using these intrinsic variables in higher-order (cubic and quartic) response surface approximations, which are highly accurate over the whole design space. To verify the high accuracy of the response surface approximations, a detailed error analysis, using an independent data set, was performed. The methodology is illustrated by constructing response surface approximations for the stresses and buckling loads of an isotropic plate with an abrupt change of thickness. These response surface approximations were then used to solve an optimization problem, where the optimal solutions are presented as a design chart.

II. Overview of Response Surface Methodology

Response surface methodology provides an approximate relationship between a response (the dependent variable) η and a vector $\boldsymbol{z}$ of k predictor variables (the independent variables). The response is generally obtained from experiments (possibly numerical), and η is the mean or expected response. The experimentally obtained response y differs from the expected value η due to random experimental error δ. The relation between y and the predictor variables is

$$y = \eta + \delta = F(z_1, z_2, \ldots, z_k) + \delta \tag{1}$$

where F is the exact dependence of η on the vector $\boldsymbol{z}$. If a response surface f is used to approximate F, Eq. (1) may be written as

$$y = f(z_1, z_2, \ldots, z_k) + \varepsilon \tag{2}$$

where ε denotes the total error, which is the difference between the predicted and the expected response values, and includes both the random (variance) error δ and the modeling (bias) error $(F - f)$. The approximating function f is normally chosen to be a low-order polynomial, and the estimated response vector at n data points $\hat{\boldsymbol{y}}$ may be written in matrix form as

$$\hat{\boldsymbol{y}} = \boldsymbol{X}\hat{\boldsymbol{\lambda}} \tag{3}$$

where the caret denotes estimated values. In Eq. (3), $\boldsymbol{X}$ is a matrix of model terms (usually monomials) evaluated at the data points. The vector $\hat{\boldsymbol{\lambda}}$ contains the unknown coefficients, which are usually estimated to minimize the sum of the squares of the error (SSE) terms, which is a process known as regression.

The response model usually includes redundant parameters or parameters poorly characterized by the experiments. These parameters may increase the error of the model and, thus, decrease its predictive capabilities (Ref. 12, p. 641, and Ref. 13). Here, redundant parameters are eliminated by mixed backward stepwise regression, e.g., see Ref. 12, pp. 642–655, and Ref. 14. Mallow's Cp statistic is used to identify the best reduced model from the subset of reduced models provided by the stepwise regression procedure and is defined as

$$Cp = \left(\mathrm{SSE}_p \big/ s_\varepsilon^2\right) - (n - 2p) \tag{4}$$

where SSE_p is the sum of the squares of the n errors for a model with p parameters (including the intercept or constant parameter) and s_ε^2 is the mean SSE terms obtained from the response model with all parameters included.

Two independent data sets and various statistical criteria are used to evaluate the predictive capabilities of the response surface approximations. Data set 1 contains all points used in constructing the response surface approximations, whereas data set 2 is an independent test set. For data set 1, the coefficient of determination R^2 statistic, the adjusted R^2 (Adj-R^2) statistic, the percent root mean square error (%RMSE), and the percent root mean square error based on the predicted sum of squares (PRESS) statistic ($\%\mathrm{RMSE}_{\mathrm{PRESS}}$) are calculated (Ref. 12, pp. 45–47). The R^2 statistic is the proportion of the variability in the response that is accounted for by the response model and has a value between 0 and 1. The adjusted coefficient of determination Adj-R^2 statistic is an alternative measure of the variability accounted for by the response model that, unlike R^2, has the desirable property that its value does not necessarily increase when adding (possibly redundant) parameters to a response surface approximation.

Percentage errors are defined in relation to the average value $\bar{y}$ of the measured response, where

$$\bar{y} = \frac{1}{n}\sum_{i=1}^{n} |y_i| \tag{5}$$

and the %RMSE is defined as

$$\%\mathrm{RMSE} = \frac{100}{\bar{y}}\sqrt{\frac{1}{\chi}\sum_{i=1}^{n}(y_i - \hat{y}_i)^2} \tag{6}$$

where $\chi = (n - p)$ for data set 1 and $\chi = n$ for data set 2. For data set 1, the %RMSE may also be defined based on the PRESS[12] statistic. For data set 2, the percent average error (%AvErr) is also calculated as

$$\%\mathrm{AvErr} = \frac{100}{n\bar{y}}\sum_{i=1}^{n} |y_i - \hat{y}_i| \tag{7}$$

and the percent maximum error (%MaxErr) is

$$\%\mathrm{MaxErr} = \max_i [(100/\bar{y})|y_i - \hat{y}_i|] \tag{8}$$

III. Plate with Thickness Change

Constructing design charts using response surface methodology is demonstrated by an example of an isotropic plate with a change in thickness in the form of a ramp (Fig. 1). The plate is simply supported on two of its edges, free on the other two edges, and subjected to a uniformly distributed load, applied on the two simply supported edges. Three nondimensional parameters, α, β, and γ, specify the geometry and location of the change in thickness (Fig. 2). Note that the definitions of β and γ are different from definitions used by Venter et al.[11] Here these variables are nondimensionalized

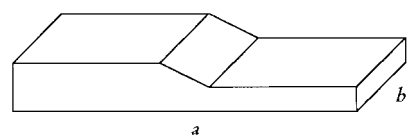

Fig. 1 Three-dimensional view of a plate with a thickness change.

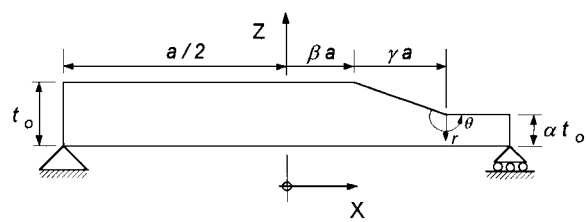

Fig. 2 Cross-sectional model with nondimensional variables shown.

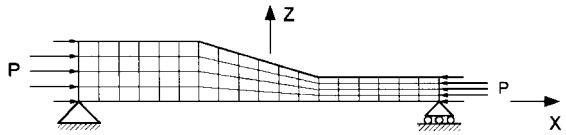

Fig. 3 Schematic finite element model used to determine the stress distribution near the re-entrant corner (actual model has about 16,000 elements).

with respect to the length a instead of the thickness t_0 as used in Ref. 11. This new definition has the advantage that all three nondimensional variables are bounded ($\alpha \in [0, 1]$, $\beta \in [-0.5, 0.5]$, and $\gamma \in [0, 1]$).

Response surface approximations for the stress distribution near the re-entrant corner and for the buckling load were constructed in terms of the geometry and location of the change in thickness. Numerical experiments were conducted using finite element models of the plate with MSC/NASTRAN Version 68. A cross section of the plate was used to model the stress distribution near the re-entrant corner, using four-node, isoparametric, plane strain elements. All models had a uniform finite element mesh, typically having 1800 elements in the x direction and 9 elements in the z direction. The number of elements varied slightly from model to model. A schematic representation of the finite element model used is shown in Fig. 3.

For buckling, four-node, isoparametric, plate bending elements were used to construct a two-dimensional 20 element × 20 element finite element model similar in shape to a plan view of Fig. 1. The eccentricity of the midplane associated with the thickness change was found to have an insignificant effect on the Euler buckling load value and was ignored in the analysis. (The eccentricity is expected to cause large deflections when the applied load approaches the buckling load value, which results in a stress failure.)

IV. Nondimensionalization

By reducing the number of variables in a response model, the accuracy and the usefulness of the model are increased. The number of variables in the response model is reduced by using variables that are intrinsic to the problem, which are identified by performing a nondimensional analysis of the governing equations.

Stress Distribution Near the Re-Entrant Corner of the Plate

The theoretical value of the stress at the re-entrant corner is infinite. Because of yielding and the impossibility of manufacturing an absolutely sharp corner, the actual stress at the corner will be finite. To account for yielding, the Von Mises criterion is used to define failure in terms of a maximum allowable yield zone near the re-entrant corner, with failure occurring when the plate yields outside of this zone. For plane strain, the radial stress at a distance r from the re-entrant corner with angle θ (see Fig. 2) is[15]

$$\sigma \sim r^{\zeta - 1} \tag{9}$$

where ζ is determined from the following transcendental equation:

$$\sin(\zeta\theta) = \pm\zeta \sin(\theta) \tag{10}$$

To avoid the need for repetitively solving Eq. (10), a third-order polynomial approximation of ζ as a function of θ (in radians) was constructed. To obtain the following equation, 19 ζ values corresponding to equally spaced values of θ between π and $3\pi/2$ were used:

$$\zeta = 7.457 - 4.046\theta + 0.8061\theta^2 - 0.05491\theta^3 \tag{11}$$

The %MaxErr [Eq. (8)] for the data points used to construct the approximation is 0.41%.

The plane strain governing equations, obtained from the equilibrium equations, and the stress–strain and strain–displacement relationships[16] depend on nine parameters: α, β, γ, a, b, t_0, P, E, and ν (see Fig. 2). By defining the nondimensional parameters

Table 1 Nondimensional boundry conditions

Boundary	Prescribed stress		Normal stress	Surface shear
$\tilde{x} = -\frac{1}{2}$	$\tilde{\sigma}_x = -\alpha$	$\tilde{\tau}_{xz} = 0$		
$\tilde{x} = \frac{1}{2}$	$\tilde{\sigma}_x = 1$	$\tilde{\tau}_{xz} = 0$		
$\tilde{z} = 0$	$\tilde{\sigma}_z = 0$	$\tilde{\tau}_{xz} = 0$		
$\tilde{z} = 1$	$\tilde{\sigma}_z = 0$	$\tilde{\tau}_{xz} = 0$		
$\tilde{z} = \alpha$	$\tilde{\sigma}_z = 0$	$\tilde{\tau}_x = 0$		
$(\frac{1}{2} + \beta) \le \tilde{x} \le (\frac{1}{2} + \beta + \gamma)$ and $\tilde{z} = m\tilde{x} + c$ $m = -(1 - \alpha)/\gamma$ $c = (1 - \alpha + 2\beta - 2\alpha\beta + 2\gamma)/2\gamma$			$\tilde{\sigma}_N = 0$	$\tilde{\tau}_S = 0$

$$\tilde{x} = x/a, \qquad \tilde{z} = z/t_0, \qquad \tilde{u} = (Et_0/P)u$$

$$\tilde{v} = (Ea/P)v, \qquad \tilde{\varepsilon}_x = (Eat_0/P)\varepsilon_x, \qquad \tilde{\sigma}_x = (\alpha bt_0/P)\sigma_x \tag{12}$$

$$\tilde{\varepsilon}_z = (Eat_0/P)\varepsilon_z, \qquad \tilde{\sigma}_z = (\alpha bt_0/P)\sigma_z$$

$$\tilde{\gamma}_{xz} = (Eat_0/P)\gamma_{xz}, \qquad \tilde{\tau}_{xz} = (\alpha bt_0/P)\tau_{xz}$$

the governing equations may be written in nondimensional form as

$$\begin{aligned} 2(1-\nu)(t_0/a)\tilde{u}_{,\tilde{x}\tilde{x}} + (t_0/a)\tilde{v}_{,\tilde{x}\tilde{z}} + (1-2\nu)(a/t_0)\tilde{u}_{,\tilde{z}\tilde{z}} &= 0 \\ (a/t_0)\tilde{u}_{,\tilde{x}\tilde{z}} + (1-2\nu)(t_0/a)\tilde{v}_{,\tilde{x}\tilde{x}} + 2(1-\nu)(a/t_0)\tilde{v}_{,\tilde{z}\tilde{z}} &= 0 \end{aligned} \tag{13}$$

The associated nondimensional boundary conditions are summarized in Table 1.

From Eq. (13) and Table 1, α, β, γ, a/t_0, and ν are identified as the intrinsic variables associated with the plane strain solution. However, the stress distribution near the re-entrant corner also depends on the radial distance measured from the corner [see Eq. (9)]. Investigations of several plate configurations showed that the maximum stress occurs on the top surface of the thinner part of the plate, where σ_x is the only nonzero stress component, and the Von Mises failure criterion reduces to

$$\tilde{\sigma}_x \ge \tilde{\sigma}_Y = \alpha bt_0\sigma_Y/P \tag{14}$$

where σ_Y denotes the material yield stress. By defining the nondimensional distance

$$\tilde{r} = r/t_0 \tag{15}$$

the response surface approximation of the nondimensional stress distribution on the top surface of the thinner part of the plate may be approximated as

$$\tilde{\sigma}_x = C_1(\alpha, \beta, \gamma) + C_2(\alpha, \beta, \gamma)\tilde{r}^{\zeta - 1} \tag{16}$$

where ζ also depends on α, γ, and a/t_0 through the angle θ. The unknown functions C_1 and C_2 in Eq. (16) are obtained by making use of response surface methodology.

Thus, there are seven intrinsic variables (α, β, γ, a/t_0, ν, $\tilde{r}$, and ζ) associated with the solution for the stress distribution near the re-entrant corner. However, it is expected that the nondimensional stress distribution varies only for small values of a/t_0 (thick plates) and that, for large a/t_0 values (thin plates), the influence of a/t_0 may be ignored. Additionally, it is anticipated that small changes in Poisson's ratio about the baseline value of 0.3 should not have a large influence on the nondimensional stress distribution. For the case where $\alpha = 0.5$, $\beta = 0$, $\gamma = 0$ (corresponding to $\theta = 3\pi/2$ and $\zeta = 0.55$), and $\tilde{r} = 0.1$ (10% of t_0), varying a/t_0 between 1 and 400 changes the nondimensional stress by less than 1% for a/t_0 larger than 25. Furthermore, for the case where $\alpha = 0.5$, $\beta = 0$, $\gamma = 0$, $\tilde{r} = 0.03$, and $\zeta = 0.55$, varying the value of ν from 0.2 to 0.4 changes the nondimensional stress by only 1.85%. In addition to these evaluations of a single design point, random combinations of α, β, and γ were evaluated (discussed in Sec. VI).

Hence, when $\nu \approx 0.3$ and $a/t_0 \geq 25$, the $\tilde{\sigma}_x$ stress on the top surface of the thin part of the plate may be described in terms of only four predictor variables, α, β, γ, and $\tilde{r}^{\zeta-1}$, where $\tilde{r}$ and ζ are combined into a single variable $\tilde{r}^{\zeta-1}$. (Predictor variables are the variables of the response model used to approximate $\tilde{\sigma}_x$.)

Buckling Load of the Plate

The buckling load of the plate depends on eight parameters: α, β, γ, a, b, t_0, E, and ν. The flexural stiffness of the plate is given by

$$D = \frac{Et^3}{12(1-\nu^2)} \tag{17}$$

where the thickness t is a function of t_0, α, β, r, and x. The nondimensional parameters

$$\tilde{x} = \frac{x}{a}, \qquad \tilde{y} = \frac{y}{a}, \qquad \tilde{t} = \frac{t}{a}, \qquad \tilde{w} = \frac{w}{a}$$
$$\tilde{N}_x = \frac{N_x}{P_{\text{Euler}}}, \qquad \tilde{D} = \frac{D}{Ea^3} = \frac{\tilde{t}^3}{12(1-\nu^2)} \tag{18}$$

are defined, and

$$P_{\text{Euler}} = \pi^2 \bar{D}/a^2 \tag{19}$$

where $\bar{D}$ is a representative value of D, described subsequently in Eq. (23). The governing equation and boundary conditions for the buckling load due to uniform axial compression[17] may be nondimensionalized to obtain

$$(\tilde{D}\tilde{w}_{,\tilde{x}\tilde{x}})_{,\tilde{x}\tilde{x}} + 2(\tilde{D}\tilde{w}_{,\tilde{x}\tilde{y}})_{,\tilde{x}\tilde{y}} + (\tilde{D}\tilde{w}_{,\tilde{y}\tilde{y}})_{,\tilde{x}\tilde{x}} - \nu(\tilde{D}\tilde{w}_{,\tilde{y}\tilde{y}})_{,\tilde{x}\tilde{x}}$$
$$- \nu(\tilde{D}\tilde{w}_{,\tilde{x}\tilde{x}})_{,\tilde{y}\tilde{y}} + 2\nu(\tilde{D}\tilde{w}_{,\tilde{x}\tilde{y}})_{,\tilde{x}\tilde{y}} = -\pi^2 \tilde{D}\tilde{N}_x \tilde{w}_{,\tilde{x}\tilde{x}} \tag{20}$$

For $\tilde{x} = -a/2$ and $a/2$,

$$\tilde{w} = 0, \qquad \tilde{w}_{,\tilde{x}\tilde{x}} = 0 \tag{21a}$$

For $\tilde{y} = -b/2a$ and $b/2a$,

$$\tilde{w}_{,\tilde{y}\tilde{y}} + \nu\tilde{w}_{,\tilde{x}\tilde{x}} = 0, \qquad \tilde{w}_{,\tilde{y}\tilde{y}\tilde{y}} + (2-\nu)\tilde{w}_{,\tilde{x}\tilde{x}\tilde{y}} = 0 \tag{21b}$$

The value of $\tilde{N}_x$ corresponding to the buckling load is $\tilde{N}_{\text{crit}}$. Five intrinsic variables associated with the solution of the buckling load are identified as ν, a/b, α, β, and γ. The nondimensionalization of Eq. (18) is based on the Euler buckling load of the plate. The nondimensional buckling load is independent of Poisson's ratio and of a/b because the Euler buckling load is independent of these parameters. However, for large values of a/b, the structure behaves like a beam rather than a plate, with the buckling load being higher by a factor of $1/(1-\nu^2)$. The dependence of the nondimensional buckling load on the variables ν and a/b was tested by varying these parameters for the case with $\alpha = 0.5$, $\beta = 0$, and $\gamma = 0$. It was found that $\tilde{N}_{\text{crit}}$ changes by 3.90% when ν is varied from 0.2 to 0.4 ($a/b = 1$), whereas $\tilde{N}_{\text{crit}}$ changes by 7.5% when a/b is varied from 0.5 to 10 ($\nu = 0.3$). Note that the relatively large error of 7.5% is because the structure behaves as a beam when $a/b = 10$. Additional evaluations of the magnitude of the dependence of the bucking load on Poisson's ratio and on a/b at other random points are described in Sec. VI. Hence, for a plate with a Poisson's ratio value close to 0.3, the response model for $\tilde{N}_{\text{crit}}$ has only three predictor variables, α, β, and γ.

V. Construction of the Response Surface Approximations

The design space and initial response surface approximations are defined in this section for the predictor variables of the response surface approximations identified in the preceding section.

Design Space

The predictor variables for the buckling load are α, β, and γ, whereas the stress distribution near the re-entrant corner introduces the additional variable $\tilde{r}^{\zeta-1}$. Response surface approximations are constructed for a wide range of α, β, γ, and $\tilde{r}^{\zeta-1}$ values, as shown in Table 2.

Table 2 Ranges of predictor variables

Predictor variable	Range
α	$0.2 \leq \alpha \leq 1.0$
β	$-0.475 \leq \beta \leq 0.475$
γ	$0 \leq \gamma \leq 0.475 - \beta$
$\tilde{r}^{\zeta-1}$	$0 \leq \tilde{r} \leq 0.8\alpha$

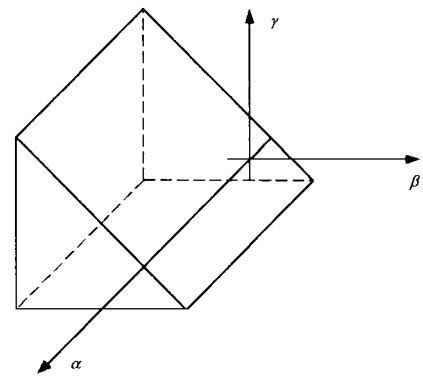

Fig. 4 Three-dimensional representation of the design space.

The upper limit on $\tilde{r}$ limits the radius of the yield zone near the re-entrant corner to be no greater than 80% of the thickness of the thin part of the plate. The upper bound on γ is dictated by the geometry of the transition region. The design space formed by α, β, and γ has a prism or wedge-like shape, as shown in Fig. 4.

Initial Response Models

Most response surface approximation applications create quadratic models, which are valid over a limited region in the design space. In the present paper, higher-order polynomials were considered with the aim of obtaining an approximation valid over the entire design space.

The behavior of the stress distribution near the re-entrant corner of the plate was determined by varying each of the four predictor variables individually for specific combinations of the other three variables. It was determined that a fourth-order polynomial in the four predictor variables (70 parameters) was suitable for an initial response surface approximation.

The buckling load response surface approximation was similarly investigated, and the resulting graphs indicate that the behavior of the buckling load response function is more complex than that of the stress distribution response function. The additional complexity is mainly due to the presence of two buckling modes. A local buckling mode is active for high slenderness ratios of the thin part of the plate, whereas a global buckling mode is active otherwise. To model these two buckling modes accurately, it is necessary to construct two independent response surface approximations, one for each buckling mode. This necessity implies that the data must be divided into two groups, corresponding to the two buckling modes. A simple geometric criterion, which assigns data points to the appropriate buckling response surface approximation, was defined based on the slenderness ratio of the thin part of the plate. This criterion is written in nondimensional form as

$$\text{buckling mode} = \begin{cases} \text{local mode} & \text{if } \dfrac{(0.5-\beta-\gamma)}{\alpha} \geq 0.6 \\ \text{global mode} & \text{if } \dfrac{(0.5-\beta-\gamma)}{\alpha} \leq 0.6 \end{cases} \tag{22}$$

With the two buckling modes defined, the value of $\bar{D}$ used for the Euler buckling load in Eq. (19) is defined as

$$\bar{D} = \begin{cases} \dfrac{E(\alpha t_0)^3}{12(1-\nu^2)} & \text{if local buckling mode} \\ \dfrac{E(t^3)_{\text{av}}}{12(1-\nu^2)} & \text{if global buckling mode} \end{cases} \tag{23}$$

After investigating several different orders of polynomials, it was determined that a third-order polynomial (20 parameters) is suitable for representing the response surface approximation for the local buckling mode and that a fourth-order polynomial (35 parameters) is suitable for representing the response surface approximation for the global buckling mode.

Estimation of the Regression Coefficients

Numerical experiments were conducted for a three-dimensional grid of equally spaced data points, with eight data points in each of the α, β, and γ directions. For a box-like domain, this procedure would yield a total of 512 data points. Because of the prism or wedge-like shape of the response surface (see Fig. 4), only 288 of these 512 data points fall within the design space.

For the stress distribution, each of the 288 plate configurations (corresponding to 288 finite element analyses) included a number of data points with different $\tilde{r}^{\zeta-1}$ values (corresponding to different finite elements). The α, β, γ, $\tilde{r}^{\zeta-1}$, and stress values for all finite elements on the top surface of the thin part of the plate were recorded for locations within 80% of the thickness of the thin part of the plate, measured from the re-entrant corner. This process yielded a total of 3023 data points, which were divided into two groups by assigning a random number between 0 and 1 to each data point. Data points with a random number less than 0.7 were allocated to the set of data points used to construct the response model, yielding 2124 data points. The remaining 899 data points were reserved to evaluate the predictive capabilities of the model.

For representing the buckling load, Eq. (22) was used to divide the 288 data points into 126 data points assigned to the construction of the local buckling mode response surface approximation and 162 data points assigned to the global buckling mode response surface approximation. An additional set of 196 data points were generated to be equally spaced, midway between the existing 288 data points, with 83 of these data points used for evaluating the local buckling mode response surface approximation and the remaining 113 data points used for evaluating the global buckling mode response surface approximation.

VI. Response Surface Approximation Accuracy

Stress Distribution near the Re-Entrant Corner

Using the mixed stepwise regression procedure,[12] the optimum number of parameters in the reduced response surface approximation for the stress distribution was found to be 43. Using both data set 1 and data set 2, the predictive capabilities of the initial response surface approximation and of the reduced response surface approximation can be compared by studying the results shown in Table 3.

The results in Table 3 indicate that both response surface approximations have similar predictive capabilities. The reduced response surface approximation is slightly more accurate (except for the %MaxErr) and is preferred because it represents a smoother function due to a smaller number of parameters. The error terms obtained from data set 1 are slightly optimistic because they are calculated from data points used to construct the response surface approximation. However, the results obtained from the $\%\mathrm{RMSE}_{\mathrm{PRESS}}$ statistic compare well with the results obtained from data set 2. This trend is a general trend when the number of data points is much larger that the number of parameters in the response surface approximation. The excellent accuracy of the reduced response surface approximation is shown graphically in Fig. 5.

The ability of the response surface approximation to predict accurate values of Poisson's ratios that are different from 0.3 was evaluated with 10 random combinations of α, β, and γ. The values $\nu = 0.25$ and 0.35 were used for each configuration. The average error for this evaluation set was 3.3%, indicating that small changes in Poisson's ratio do not affect the results.

An important and desirable characteristic of response surface approximations is their tendency to filter out numerical noise. This characteristic is illustrated for the maximum stress value on the top surface of the thin part of the plate (independent of $\tilde{r}$) as a function of α for $\beta = \gamma = 0$. These values of β and γ correspond to a sharp transition at the midlength of the plate. For this illustration, 60 data points were evaluated, and the results are shown in Fig. 6. Also

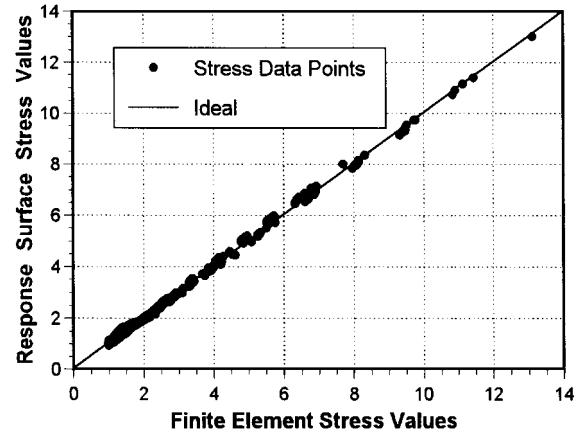

Fig. 5 Comparison of response surface approximation and finite element nondimensional stress results: data sets 1 and 2.

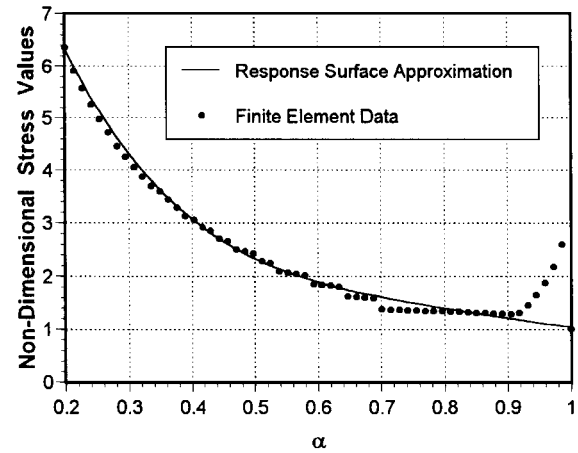

Fig. 6 Maximum nondimensional stress value as a function of α ($\beta = 0, \gamma = 0$).

shown in Fig. 6 is the response obtained from the corresponding response surface approximation.

There are some inconsistencies in the data obtained from the finite element model, which may be attributed to the mesh generation procedure that did not provide finite element models with a consistent level of fidelity. In particular, it yielded less accurate finite element models when γ is equal to 0 and α is close to 1 (which corresponds to a sharp transition with a small change in thickness). The results presented in Fig. 6 indicate that the response surface approximation eliminated these inconsistencies, or noise, and that not all differences between predicted and numerical response values should be considered to be errors. For some cases, the predicted response values may indeed be more accurate than the numerical response values, as is the case in Fig. 6 when α is close to 1. When α is close to 1, the nondimensional finite element stress values should approach a value equal to 1 and are, thus, in error. The problem associated with the mesh generator disappears when α is equal to 1 (no change in thickness) because the nondimensional finite element stress value for this point is also equal to 1 (thus no stress concentration).

Buckling Load

Using the mixed stepwise regression procedure,[12] the best reduced response surface approximation for the local buckling load (cubic polynomial) has 19 parameters, whereas the reduced response surface approximation for the global buckling load (quartic polynomial) has 25 parameters.

The accuracy of the results predicted with the response surface approximations is summarized in Tables 4 and 5, and a graphical representation of the accuracy of the reduced response surface approximations is shown in Fig. 7. In addition, to determine the accuracy of the response surface approximations for different values of ν and a/b, 10 random combinations of α, β, and γ were evaluated

Table 3 Response surface approximation for the stress distribution

	Data set 1 (2124 points)					Data set 2 (899 points)		
Stress model	Cp	R^2	Adj-R^2	%RMSE	%RMSE$_{PRESS}$	%AvErr	%RMSE	%MaxErr
Full (70 terms)	70	0.9984	0.9983	3.2478	3.4172	2.4552	3.5934	16.443
Reduced (43 terms)	31.927	0.9983	0.9982	3.2964	3.3886	2.4339	3.4754	17.120

Table 4 Response surface approximation for local buckling mode

	Data set 1 (126 points)					Data set 2 (83 points)		
Model	Cp	R^2	Adj-R^2	%RMSE	%RMSE$_{PRESS}$	%AvErr	%RMSE	%MaxErr
Full (20 terms)	20	0.9999	0.9998	0.5541	0.6927	0.7056	0.9567	2.8494
Reduced (19 terms)	19.402	0.9999	0.9998	0.5550	0.6920	0.7055	0.9598	2.8792

Table 5 Response surface approximation for global buckling mode

	Data set 1 (126 points)					Data set 2 (113 points)		
Model	Cp	R^2	Adj-R^2	%RMSE	%RMSE$_{PRESS}$	%AvErr	%RMSE	%MaxErr
Full (35 terms)	35	0.9912	0.9889	2.5538	3.1695	1.1998	1.6895	5.4340
Reduced (25 terms)	18.122	0.9910	0.9895	2.4888	3.0202	1.1936	1.6935	5.8767

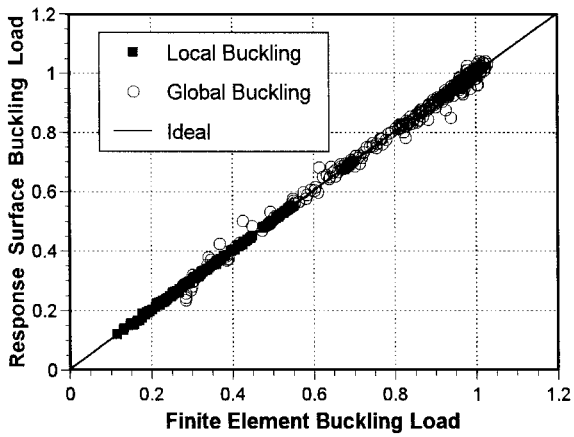

Fig. 7 Comparison of nondimensional buckling loads from response surface approximations and finite element analysis for local and global buckling modes: data sets 1 and 2.

for $\nu = 0.25$ and 0.35 and for $a/b = 0.1$ and 5. For $a/b = 0.1$, the average error is 4.5%, and for $a/b = 5$, the average error ranges from 2.7% for $\nu = 0.25$ to 9.1% for $\nu = 0.35$. This larger error reflects that the structure behaves like a beam rather than a plate for $a/b = 5$.

As was the case for the stress distribution response surface approximation, both the reduced and the full response surface approximations provide similar predictive capabilities. As before, the reduced response surface approximations are preferred over the full response surface approximations and will be used for the optimization problem described in the next section.

VII. Optimization Problem

To demonstrate the use of the developed response surface approximations for optimization problems, a steel plate was considered with the material, geometric, and load parameters summarized in Table 6.

The objective of the optimization problem is to find the geometry and location of the change in thickness that minimize the weight of the plate, without yielding or buckling of the plate. Fixed values of α and a/t_0 were used for the optimization problem. These fixed values correspond to the design problem of finding the geometry and location of the change in thickness when the thicknesses of the thick and thin parts are specified.

Table 6 Parameters of the example problem

Variable	Value
E	30×10^6 psi
ν	0.29
σ_y	30×10^3 psi
a	90 in.
b	45 in.
t_0	2 in.
αt_0	0.7 in.
P	400,000 lb

Table 7 Nondimensional input parameters of the optimization problem

Variable	Value
α	0.35
a/t_0	45
$\tilde{\sigma}_y$	2.3625
$\tilde{N}_x$	7.7920
$\tilde{r}$	0.05α

By using a nondimensional formulation of the optimization problem, the number of input parameters is minimized, and it is possible to solve the problem using only five nondimensional parameters. All input parameters, except for the allowable yield zone $\tilde{r}$, are taken from the properties as summarized in Table 6 and are shown in Table 7. The allowable yield zone was assumed to be 5% of the thickness of the thin part of the plate. Throughout the optimization problem, the axial load N_x and the buckling load N_{crit} are nondimensionalized with respect to the Euler buckling load of a plate with a constant thickness equal to αt_0.

The Microsoft Excel solver implemented in Microsoft Excel Version 7.0 was used to find the optimum solution. This software employs a generalized reduced gradient algorithm and approximates the required derivatives numerically using forward differences.

The nondimensional formulation of the optimization problem is as follows:

Minimize the plate cross-sectional area given by

$$\tilde{A} = A/at_0 = \tfrac{1}{2}(1 + 2\beta + \gamma) + (\alpha/2)(1 - 2\beta - \gamma) \qquad (24)$$

Table 8 Optimum solution

β	γ	Area
−0.1526	0.6276	0.7798

Table 9 Comparison with FE results

Method	$\tilde{N}_{\text{crit}}$	$\tilde{\sigma}_{x(\tilde{r}=0.05\alpha)}$
RSM	7.7920	0.9977
FE	7.5645	1.1207
% Difference	2.92	10.98

Subject to

$$\frac{\beta}{0.475}+1\geq 0, \qquad \frac{\beta}{0.475}-1\leq 0$$
$$\gamma\geq 0, \qquad \frac{\gamma+\beta}{0.475}-1\leq 0 \tag{25}$$
$$\frac{\tilde{\sigma}_{x(\tilde{r}=0.05\alpha)}}{\tilde{\sigma}_y}-1\leq 0, \qquad \frac{\tilde{N}_{\text{crit}}}{\tilde{N}_x}-1\geq 0$$

where $\tilde{\sigma}_x=\tilde{\sigma}_x(\alpha,\beta,\gamma,\tilde{r}^{\zeta-1})$, with $\zeta=\zeta(\alpha,\gamma,a/t_0)$, and where $\tilde{N}_{\text{crit}}=\tilde{N}_{\text{crit}}(\alpha,\beta,\gamma)$ are obtained from the constructed response surface approximations, $\tilde{\sigma}_Y=\tilde{\sigma}_Y(\alpha,\beta,t_0,P,\sigma_Y)$ [see Eq. (14)] and $\tilde{N}_x=\tilde{N}_x(\alpha,a,t_0,P,\nu,E)$ [see Eqs. (18) and (23)].

The reduced response surface approximations were used throughout the optimization process. A total of 10 initial design points were used, 1 at each vertex of the two-dimensional, triangular design space, 1 at the center of the design space, and the remaining 6 randomly distributed throughout the design space. No local minima were found, and the optimum design point is summarized in Table 8.

The critical constraints for the optimum solution were the constraints relating the upper limits of β and γ and the global buckling load constraint. The optimum solution corresponds to a gradual change in thickness, starting well left of the midlength of the plate and continuing to the rightmost endpoint (see Fig. 2). For the example problem ($a/t_0=45$), the buckling load constraint dominates the solution. However, as a/t_0 is reduced, the solution of the optimization problem first moves into a region of the design space where both the buckling load and yield stress constraints are active and then into a region where only the yield stress constraint is active.

To validate the accuracy of the optimum solution, the stress distribution and buckling load values predicted by the response surface methodology (RSM) were compared with results obtained from the finite element (FE) analyses (Table 9). The differences between the results are 2.92 and 10.98%, respectively.

Finally, the example problem may be extended to demonstrate the true generality of the solution process. By determining numerical optimization solutions for different values of α, $\tilde{\sigma}_Y$, and $\tilde{N}_x$, it is possible to construct two new response surface approximations: 1) a response surface approximation that relates the optimum solution $\tilde{A}$ to α and $\tilde{\sigma}_Y$ and 2) a response surface approximation that relates the optimum solution $\tilde{A}$ to α and $\tilde{N}_x$. The first response surface approximation corresponds to an optimization problem where the buckling load constraint is removed, and the second response surface approximation corresponds to an optimization problem where the yield stress constraint is removed. For each response surface approximation, 105 data points were evaluated, and different values of $\tilde{\sigma}_Y$ and $\tilde{N}_x$ were obtained by varying $\alpha\in[0.2, 1.0]$ and $P\in[25{,}000, 1{,}100{,}000]$ lb.

In each case, the results were divided into two groups: a set of data points where the failure mode considered is inactive (case 1) and a set of data points where the failure mode considered is active (case 2). Case 1 corresponds to a small applied load that results in the minimum area [Eq. (24) with $\beta=-0.475$ and $\gamma=0$]. For each of the two response surface approximations, the data points of case 2 were used to construct the corresponding response surface approximations. For both response surface approximations, bilinear initial models (four parameters) were used. In each case, the initial response surface approximations were reduced to only three parameters using mixed stepwise regression. The reduced response surface approximations are given by

$$\tilde{A}_{\text{YS}}^{\text{OptPred}}=\max\begin{cases}0.025+0.975\alpha\\ 0.5095+0.6555\alpha-0.1801898\alpha\tilde{\sigma}_Y\end{cases} \tag{26}$$

$$\tilde{A}_{\text{BL}}^{\text{OptPred}}=\begin{cases}0.025+0.975\alpha & \text{if } \tilde{N}_x<1\\ 0.2795+0.0113\tilde{N}_x^{\frac{1}{3}}+0.6714\alpha\tilde{N}_x^{\frac{1}{3}} & \text{otherwise}\end{cases}$$

where the predicted, nondimensional plate cross-sectional area is $\tilde{A}_{\text{YS}}^{\text{OptPred}}$ when only the yield stress constraint is considered and is $\tilde{A}_{\text{BL}}^{\text{OptPred}}$ when only the buckling load constraint is considered. The two response surface approximations of Eq. (26) are shown graphically in Figs. 8 and 9.

The effect of the change from the inactive (case 1) to the active failure constraint is shown in Figs. 8 and 9, where the graphs change from a horizontal line to an inclined line. The design charts in Figs. 8 and 9 are valid only for $a/t_0=45$, but it is possible to construct a series of similar design charts for different a/t_0 values.

The accuracy of the results predicted with the reduced response surface approximations is summarized in Table 10. Because only

Table 10 Response surface approximation for the optimal area

Constraint	Model	R^2	Adj-R^2	RMSE	%RMSE$_{\text{PRESS}}$
	Case 2 data points (33 points)				
Yield stress	Reduced (three terms)	0.9945	0.9942	1.3483	1.6828
	Case 2 data points (67 points)				
Buckling load	Reduced (three terms)	0.9851	0.9847	1.8127	1.8756

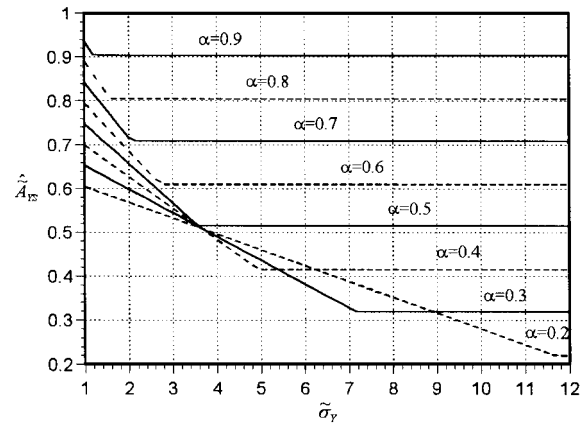

Fig. 8 Design chart for the optimum cross-sectional area as a function of α and $\tilde{\sigma}_Y$ for $a/t_0=45$.

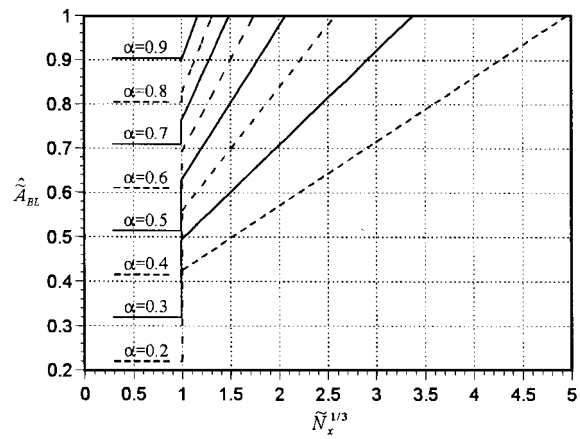

Fig. 9 Design chart of the optimum cross-sectional area as a function of α and $\tilde{N}_x^{1/3}$ for $a/t_0=45$.

Table 11 Predicted vs calculated optimum nondimensional cross-sectional area

Method	Area
RSM	0.7678
Optimum	0.7798
% Difference	1.54

a single data set was used to construct each response surface approximation, the $\%\mathrm{RMSE}_{\mathrm{PRESS}}$ statistic was used to compensate for the possibly overly optimistic error estimates. This statistic provides good results when the number of data points used to construct the response surface approximation is much larger than the number of parameters in the response surface approximation.

The final response surface approximation relating the required nondimensional area $\tilde{A}$ to α, $\tilde{\sigma}_Y$ and $\tilde{N}_x$ may be written as

$$\tilde{A}^{\mathrm{OptPred}} = \max \begin{cases} \tilde{A}_{\mathrm{YS}}^{\mathrm{OptPred}} = \tilde{A}_{\mathrm{YS}}^{\mathrm{OptPred}}(\alpha, \tilde{\sigma}_Y) \\ \tilde{A}_{\mathrm{BL}}^{\mathrm{OptPred}} = \tilde{A}_{\mathrm{BL}}^{\mathrm{OptPred}}(\alpha, \tilde{N}_x) \end{cases} \tag{27}$$

The accuracy of the response surface approximation for the optimum nondimensional plate cross-sectional area may be validated by applying Eq. (27) to the example problem of Table 7 (optimum solution shown in Table 8). The results are summarized in Table 11.

VIII. Concluding Remarks

Making use of accurate response surface approximations is a way of overcoming some of the numerical noise and software integration problems associated with solving complex engineering optimization problems. The process of obtaining an accurate response surface approximation by tailoring the response surface approximation for a specific design problem is outlined. The tailoring process involves identifying design variables that are intrinsic to the design problem by nondimensionalizing the problem, by investigating the response in the design space, and by using higher-order polynomials (cubic and quartic instead of the more traditional quadratic) as response surface approximations. Additionally, stepwise regression is used to remove insignificant parameters from the response surface approximations, and finally, an independent data set is used to perform a detailed error analysis. This process results in response surface approximations that are highly accurate over the whole design space.

The highly accurate response surface approximations obtained were successfully used to determine the minimum weight of a plate with a thickness change. A derivative-based optimization algorithm could be used for the optimization process because the response surface approximations are smooth in nature. Solving the optimization problem was computationally inexpensive and resulted in an optimum solution that demonstrated excellent correlation with finite element results.

Finally, it was shown that by making use of RSM the optimum solution may be presented in the form of a design chart that is applicable for a wide range of load and geometric parameters.

Acknowledgments

This work was supported in part by NASA Grants NAG1-1669 and NAG1-2000.

References

[1]Giunta, A. A., Dudley, J. M., Narducci, R., Grossman, B., Haftka, R. T., Mason, W. H., and Watson, L. T., "Noisy Aerodynamic Response and Smooth Approximations in HSCT Design," *Proceedings of the AIAA/NASA/USAF/ISSMO 5th Multidisciplinary Analysis and Optimization Symposium* (Panama City, FL), Pt. 2, AIAA, Washington, DC, 1994, pp. 1117–1128 (AIAA Paper 94-4376, Sept. 1994).

[2]Kaufman, M., Balabanov, V., Grossman, B., Mason, W. H., Watson, L. T., and Haftka, R. T., "Multidisciplinary Optimization via Response Surface Techniques," *Proceedings of the 36th Israel Conference on Aerospace Sciences* (Israel), Omanuth, Haifa, Israel, 1996, pp. A-57–A-67.

[3]Mason, B. H., Haftka, R. T., and Johnson, E. R., "Analysis and Design of Composite Channel Frames," *Proceedings of the AIAA/NASA/USAF/ISSMO 5th Multidisciplinary Analysis and Optimization Symposium* (Panama City, FL), Pt. 2, AIAA, Washington, DC, 1994, pp. 1023–1040 (AIAA Paper 94-4363, Sept. 1994).

[4]Tai, J. C., Mavris, D. N., and Schrage, D. P., "Application of a Response Surface Method to the Design of Tipjet Driven Stopped Rotor/Wing Concepts," *Proceedings of the AIAA 1st Aircraft Engineering, Technology, and Operations Congress* (Los Angeles, CA), AIAA, Washington, DC, 1995 (AIAA Paper 95-3965, Sept. 1995).

[5]Giunta, A. A., Balabanov, V., Burgee, S., Grossman, B., Haftka, R. T., Mason, W. H., and Watson, L. T., "Variable-Complexity Multi-Disciplinary Design Optimization Using Parallel Computers," *Computational Mechanics '95—Theory and Application*, Springer, Berlin, 1995, pp. 489–494.

[6]Brown, R. T., and Nachlas, J. A., "Structural Optimization of Laminated Conical Shells," *AIAA Journal*, Vol. 23, No. 5, 1985, pp. 781–787.

[7]White, K. P., Jr., Hollowell, W. T., Gabler, H. C., III, and Pilkey, W. D., "Simulation Optimization for the Crashworthiness of a Passenger Vehicle in Frontal Collision Using Response Surface Methodology," *SAE Transactions*, Sec. 3, Society of Automotive Engineers, Warrendale, PA, 1985, pp. 798–811.

[8]Mistree, F., Patel, B., and Vadde, S., "On Modeling Objectives and Multilevel Decisions in Concurrent Design," *Proceedings of the ASME Design Automation Conference* (Minneapolis, MN), American Society of Mechanical Engineers, New York, 1994, pp. 151–161.

[9]Van Houten, M. H., Schoofs, A. J. G., and Van Campen, D. H., "Response Surface Techniques in Structural Optimization," *Proceedings of the 1st World Congress of Structural and Multidisciplinary Optimization* (Gosler, Germany), Redwood, Trowbridge, England, UK, 1995, pp. 89–94.

[10]Thacker, B. H., and Wu, Y. T., "A New Response Surface Approach for Structural Reliability Analysis," *Proceedings of the AIAA/ASME/ASCE/AHS/ASC 33rd Structures, Structural Dynamics, and Materials Conference* (Dallas, TX), Pt. 2, AIAA, Washington, DC, 1992, pp. 586–593 (AIAA Paper 92-2408, April 1992).

[11]Venter, G., Haftka, R. T., and Starnes, J. H., Jr., "Construction of Response Surfaces for Design Optimization Applications," *Proceedings of the AIAA/NASA/ISSMO 6th Multidisciplinary Analysis and Optimization Symposium* (Bellevue, WA), Pt. 1, AIAA, Reston, VA, 1996, pp. 548–564 (AIAA Paper 96-4040, Sept. 1996).

[12]Myers, R. H., and Montgomery, D. C., *Response Surface Methodology: Process and Product Optimization Using Designed Experiments*, Wiley, New York, 1995, pp. 45–47, 641–655.

[13]Kaufman, M., Balabanov, V., Burgee, S. L., Giunta, A. A., Grossman, B., Mason, W. H., Watson, L. T., and Haftka, R. T., "Variable-Complexity Response Surface Approximations for Wing Structural Weight in HSCT Design," *Journal of Computational Mechanics*, Vol. 18, No. 2, 1996, pp. 112–126.

[14]Ott, R. L., *An Introduction to Statistical Methods and Data Analysis*, Duxbury, Belmont, CA, 1993, pp. 648–659.

[15]Williams, M. L., "Stress Singularities Resulting from Various Boundary Conditions in Angular Corners of Plates in Extension," *Journal of Applied Mechanics*, Vol. 19, Dec. 1952, pp. 526–528.

[16]Cook, R. D., Malkus, D. S., and Plesha, M. E., *Concepts and Applications of Finite Element Analysis*, Wiley, New York, 1989, pp. 20, 21.

[17]Timoshenko, S., *Theory of Elastic Stability*, McGraw–Hill, New York, 1936, pp. 297, 337–350.

A. D. Belegundu
Associate Editor